Proceedings of the 39th Chinese Control Conference
July 27-29, 2020, Shenyang, China

Numerical Analysis on Aerodynamic Interference of a Novel Tilt-rotor UAV in Transition Mode

Huaping Huang, Guang He*, Li Yu, Xiangke Wang
College of Intelligence Science and Technology,National University of Defense Technology, Changsha 410073, P. R. China
E-mail: heguang@nudt.edu.cn

Abstract: In order to investigate the aerodynamic interference of a novel tilt-rotor UAV in transition mode more effectively, numerical analysis based on CFD (Computational Fluid Dynamics) is completed in this paper. Firstly, the model of the designed UAV is introduced. For the simulations, the hybrid grid method is used to establish the UAV and background grid, the $S-A$ (Spalart-Allmaras) model is used as the model of air, and the MRF (Multiple Reference Frame) method is used to establish the rotor model. Based on the above methods, the flow fields of tilt-rotor UAV in transition mode are simulated with three-dimensional Navier-Stokes equations. Furthermore, comparisons between simulations and experiments are made to demonstrate the reliability of the proposed CFD method in simulating the flow fields of tilt-rotor UAV. After the establishment and verification of the CFD method. The analysis of the tilting curve is made to provide the method to organize the numerical simulation. By analysis and comparisons on the results of numerical simulation, some meaningful conclusions about aerodynamic interference caused by rotor/wing in the transition mode are obtained.

Key Words: Tilt-rotor UAV, Transition mode, CFD, Aerodynamic interference

1 Introduction

Tilt-rotor UAV is an aircraft that can land and take off vertically, as well as convert to airplane mode to achieve high-speed cruise performance[1]. Researchers have made great effort on the tilt-rotor UAV in recent years due to its unique advantages and technical complexity. Many successful UAVs have appeared, such as panther, firefly6 and smartUAV. The transition mode, as an important process of the tilt-rotor UAV's flight, is affected by many factors, one of which is the strong aerodynamic interference between the rotor and the wing. Along with the tilting of the rotors, the downwash purling generated by the rotor creates three-dimensional turbulent flow on the upper surface of the wing. The downward purling imposed on the wing has a significant impact on the stability in the tilt-rotor UAV's transition mode[2]. Therefore, the study on the rotor/wing aerodynamic interference is of great practical significance on the design of tilt-rotor UAV's controller design.

The existing methods of rotor/wing aerodynamic interference of tilt-rotor UAV mainly include theoretical analysis, experimental research and simulation[3]. The theoretical analysis methods mainly include momentum theory, blade-element theory and eddy current theory [4]. Reference [7] analyzed the aerodynamic interference of rotor/wing with aid of theoretical analysis, and a model for TURAC was obtained. However, when the propeller rotates, the three-dimensional turbulent flow is complicated and the theoretical calculation results cannot meet the design requirements completely. Some researchers obtain the aerodynamic characteristics of the UAV by experiments[5] in recent years. Though the experiments are more credible, whereas, the experiments means the high cost of money and time as well as high risk. With the development of computer science, low-cost and flexible computational fluid dynamics (CFD) methods have been widely used in the study of aircraft aerodynamic characteristics. Reference [8–10] used the CFD methods to analyze the flow field of isolated rotors, isolated wing and the rotor/wing/fuselage in detail. However, all of them focus on the flow field around the rotors and wing. The analysis of the impact of the flow field is inadequate.

In this paper, the aerodynamic interference between the rotors and the wing of a novel tilt-rotor UAV in transition mode is analyzed based on the CFD method. At first, the basic structure of the UAV is introduced. Then, considering the accuracy and computational efficiency, the hybrid grid and corresponding CFD solver are set to establish a complete numerical simulation system. Besides, the accuracy of the CFD is validated by the comparison between simulations and experiments. After that, the simulations are organized according to the given tilting curve. Finally, the results of the isolated wing model and rotor/wing model are analyzed to determine the impact of aerodynamic interference. Based on this, the idea to improve the accuracy of attitude control is provided.

2 Description of UAV

Fig. 1: Prototype of tilt-rotor UAV

The considered novel tilt-rotor uses five motors as the dynamical system as shown in Fig.1. All the rotors have the ability to tilt. The motors are divided into two groups. One group is made up of four motors placed on the leading edge of the wing, the other is one motor placed on the rear of the fuselage. The front four motors are connected to servos, which are connected to the wing spar through the carbon rod. The rear motor is equipped with a servo as the tilt

mechanism. When the tilt angle is 0 degrees, the front motors are vertically upward while the rear motor is vertically downward. The tilt-rotor UAV is with a bi-tail-boom layout, and the empennage is higher than the fuselage. Two vertical tails are used to connect the ends of the empennage and the carbon rods, which are attached to the lower surface of the wing. In this way, the airflow of the rear motor will not influence the empennage. Therefore only the effect of the front rotors should be considered.

The main parameters of the UAV are shown in Tab. 1.

Table 1: Basic parameters of the aircraft

Body length	2 m
Span	2.8 m
Average aerodynamic chord length	0.356 m
Root tip ratio	0.448
Wing reference area	0.95 m^2
Aspect ratio	8.3
Front propeller diameter	0.356 m
Rear propeller diameter	0.559 m

In order to keep the attitude stable, a control strategy with a slow transform is designed. The control strategy is as follows: the four front motors and the rear motor tilt at the same time to provide vertical thrust and forward thrust. The speed of the rotors' tilting is slow. Meanwhile, the tilt angle curve is used to keep the balance between the gravity and the mix of the lift and the vertical component of the rotors' thrust. In transition mode, the motors ensuring the thrust at first, then the line drive of the servos is used to help the control of attitude. The key to this control strategy is to maintain a balance of forces and moments in the vertical plane. However, due to the downwash purling of the rotor, the aerodynamic interference will influence the aerodynamic force and aerodynamic moment in the whole process of tilting. Therefore, the study on aerodynamic interference is a necessary condition for control strategy. In most cases, the experiments can provide good performance. Whereas, experiments for the whole process may cost a lot, meanwhile, experiments for a novel tilt-rotor are complex and more than aerodynamic experiments which cost lots of time. As a result, lowcost CFD method is used to obtain the aerodynamic interference of the UAV in the transition mode in this paper.

3 Numerical Methodology

3.1 Grid system

The first step of the CFD simulation for the UAV's transition mode is meshing. The continuous space needs to be divided into discretized grids to compute. The quality of the grid directly affects the accuracy and convergence of the calculation results. As a result, a set of high-quality grids should be established. Besides, considering the relative movement among different components of tilt-rotor UAV, a hybrid grid based on the structured grid and the unstructured grid is generated. At the same time, a minor calculation domain with the rotor and a background calculation domain with enclosing bodies are generated separately. The minor calculation domain is fully embedded inside the background calculation domain. The calculation domain can describe as follows(as shown in Fig.3):

(a) Five cylinders(as shown in Fig.3a) whose height is 25 times the rotor diameter and diameter is 4 times the rotor diameter are generated as the calculated domain of the rotor. In this minor calculation domain, the flow field caused by the rotor can be computed accurately.

(b) A cube(as shown in Fig.3b) with a side length of 50 times the average aerodynamic chord is generated as the background calculation domain. In this background calculation domain, the flow field of the whole tilt-rotor UAV can be computed.

In order to get the accurate forces and moments as well as considering the compute complexity, the hybrid grid is divided into four parts(as shown in Fig.4): (a) An unstructured grid is generated by free triangular grid around the surface layer of the wing. To ensure the quality of the grids, the grids are densely processed at the area where the geometric surface transition is visible. At the same time, all the grids are smoothed; (b) A boundary layer grid is generated by quadrilateral grid on the surface layer. Closing treatment near the symmetry plane is used to facilitate the setting of boundary conditions; (c) The background grid is generated by free triangle grid in the background calculation domain; (d) An unstructured grid is generated by free triangular grid around the rotor.

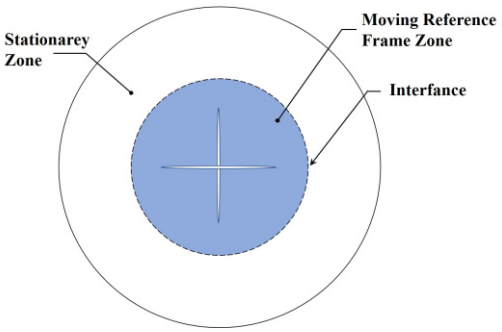

Fig. 2: MRF method

Considering the rotation of the propeller, the MRF method is used to describe the model of the rotor. As shown in the Fig.2, the MRF method divides the calculation domain into multiple small subdomains. The flow field around the propeller is in the moving reference frame zone. While the flow field outside the rotor area is in stationarey. The velocity of the flow field at the interface is the same. Meanwhile, the flow field governing equations are solved in each subdomain, and the flow field information is exchanged at the interface of the subdomains by converting the speed to absolute speed.

3.2 Governing Equations

In CFD simulation, the air is described as a viscous incompressible fluid. In this case, the Navier-Stokes equation(given as equation (1)) is suitable as the governing equation in the entire simulation process.

$$\frac{\partial}{\partial t}\int_{\Omega} W d\Omega + \oint_{\partial Q} (F_c - F_v)\cdot n ds = 0 \qquad (1)$$

Where W is a conservation variable, F_c is the nonviscous flux, and F_v is viscous flux. Their expressions are

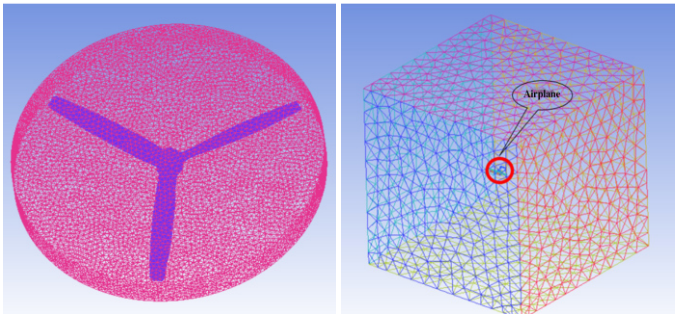

(a) Computational domain of rotor (b) Computational domain of airplane

Fig. 3: Computational domain

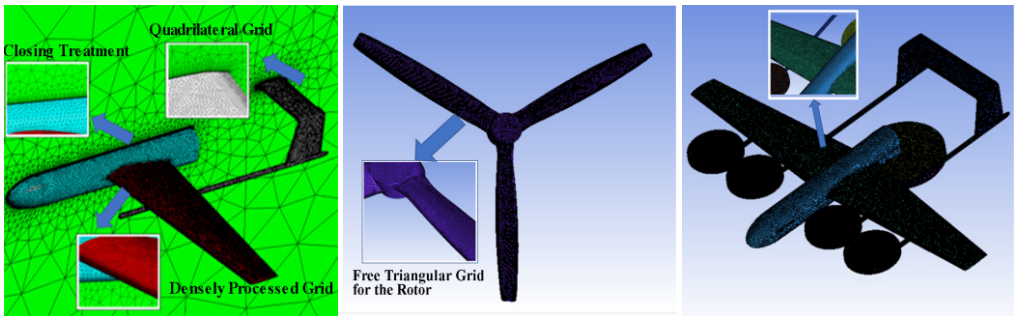

(a) Grid of half body (b) Grid of rotor (c) Grid of the whole UAV

Fig. 4: Grid system of UAV

$$F_c = [\rho V_r \quad \rho u V_r + p n_x \quad \rho v V_r + p n_y \quad \rho w V_r + p n_z \quad \rho H V_r + p V_t]^T \tag{2}$$

$$W = \begin{bmatrix} \rho & \rho u & \rho v & \rho w & \rho E 1^T \end{bmatrix} \tag{3}$$

$$F_v = \begin{bmatrix} 0 \\ \tau_{xx} n_x + \tau_{xy} n_y + \tau_{xx} n_z \\ \tau_{yx} n_x + \tau_{y} n_y + \tau_{yz} n_z \\ \tau_{zx} n_x + \tau_{zy} n_y + \tau_{zz} n_z \\ \mathbf{\Phi}_x n_x + \mathbf{\Phi}_y n_y + \mathbf{\Phi}_z n_z \end{bmatrix} \tag{4}$$

where Ω is the volume of the control unit; $\partial\Omega$ is the area of unit ; u, v, and w are the components of the absolute velocity in the coordinate system;$n = [n_x \ n_y \ n_z]^T$ is the normal vector of the surface; ρ and t is the density and time respectively; V_r is the relative speed; $V_t$is the relative speed of the grid; E and H are the total energy and total enthalpy.

3.3 Turbulence Model

The $S-A$ model is the most common single-equation model in RANS (Reynolds Average Navier-Stokes). It only refers to the transport equation of turbulent viscosity without the length dimension of the local shear layer thickness. This model is mainly used in the field of aviation for its strong robustness. It is suitable for the tilt-rotor UAV for the huge demand for correlation calculation. Meanwhile, the $S-A$ model pays more attention to the trend of the variables and the efficiency of the solution. Therefore, this paper uses the $S-A$ model. In the $S-A$ model, the eddy viscosity coefficient is:

$$\mu_t = \rho \hat{v} f_{vl} \tag{5}$$

where the transport equation of $\hat{v}$ is:

$$\frac{\partial \hat{v}}{\partial t} + u_j \hat{v}_j = C_{b1} \tilde{S} \hat{v} + \frac{1}{\sigma_{\hat{v}}} \left[\{(v + \hat{v}) \hat{v}_k\}_{,k} + C_{b2} \rho \hat{v}_{,k} \hat{v}_{,k} \right] - C_{w1} \rho f_w \left(\frac{\hat{v}}{d}\right)^2 \tag{6}$$

In this paper, the closure coefficient and approximate relationship are set according to [6].

3.4 CFD Model Validation

In order to verify the accuracy of this model, the comparison between CFD simulations and experiments is completed. The comparison is divided into two parts: one is the comparison for the aerodynamic force; the other is the comparison of the rotors' thrust.

Firstly, the comparison for the aerodynamic force beteen the wind tunnel experiment and simulation is done. In order to make the comparison, the environment in simulations such as air density, the material of UAV and turbidity of air are set the same as those in the wind tunnel. Due to the UAV system, all the results are changed into the coefficient of lift, drag, and pitch moment, which can be computed as follows:

$$C_L = \frac{2L}{\rho V^2 S}$$

$$C_D = \frac{2D}{\rho V^2 S} \tag{7}$$

$$C_m = \frac{2M}{\rho V^2 S l_1}$$

where ρ represents the atmospheric density, S represents the effective wing area of the aircraft, V represents the freestream speed, l_1 represents the average aerodynamic chord length, L represents the lift received by the aircraft,

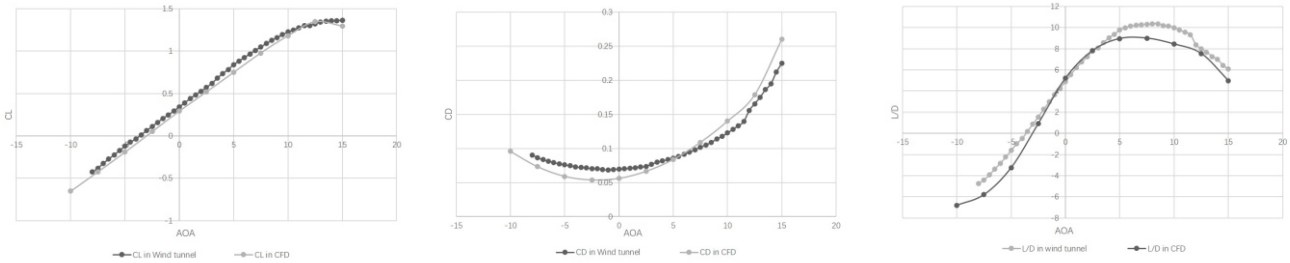

(a) CL (b) CD (c) L/D

Fig. 5: Comparisons of CFD data with wind tunnel data

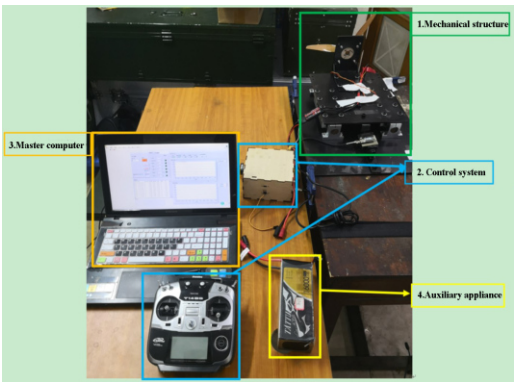

Fig. 6: Experimental system for tension force test of rotor

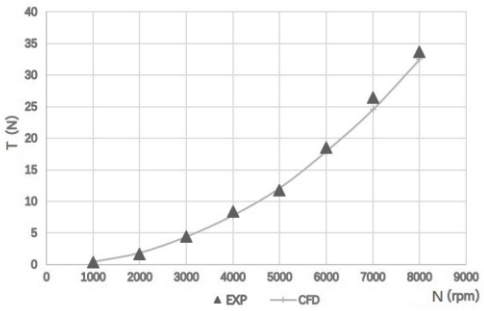

Fig. 7: Tension force of the rotor at typecal rev

and D represents the drag received by the aircraft, M represents the pitching moment received by the aircraft, and C_L, C_D, and C_M represent the lift coefficient, drag coefficient, and pitch moment coefficient of the aircraft respectively.

The results of CFD simulations and wind tunnel experiments are given in Fig.5, which shows the lift-drag ratio and the coefficient of lift and drag at 20m/s at different attack angles. It can be seen that the coefficient of lift and lift-drag ratio in CFD is close to those in wind tunnel when the attack angle is from -5 degree to 5 degree. Although, the drag has some errors with the experiments caused by the slight difference of model. The trend of the curve is the same and the errors are in the ballpark. At the same time, the expected angle of attack in transition mode is 0 degree, so we regard the results in the CFD simulation as the actual value.

In addition, the comparison of the rotors' thrust is done. The experimental system of the rotor test (as shown in Fig.6) is set up. In order to get the characteristic of the rotors, the speed of the rotor is set at 1000 RPM to 8000 RPM and the tension force is recorded. At the same time, the same condition such as the air density and the material of the rotor is set up in the CFD simulation. Fig.6 shows the results of the experiment and the CFD simulation. It can be seen that at the speed of 1000 RPM to 8000 RPM the thrust errors are tiny enough to regard the value in CFD as the actual value.

From the above two comparisons, we can conclude that the setting of the CFD is validated and the results are credible.

4 Numerical Simulation of Rotor/Wing Aerodynamic Interference

4.1 Numerical Simulation

In the process of numerical simulation of rotor/wing aerodynamic interference, it is necessary to save computing resources and speed up the simulation progress. Therefore, a preliminary tilting curve based on theoretically calculated is drawn. During the numerical simulation process, the points around the tilting curve are taken as the main reference point, and the rotation speed of the motor is set up to 7000 RPM to meet the conversion process of the UAV in transition mode and keep the reliability of results for the rotor in CFD. The tilt angle curve of theoretical calculation is shown in Fig.8, and the point in the figure is a balance point where the gravity is equal to the sum of the lift provided by the wing and the vertical thrust of the rotors. It can be seen that the UAV is work at 0 m/s to 25 m/s in transition mode. Considering the computational complexity, the experiment is organized as follows(as shown in table 2): firstly, we set the speed of the UAV at 5 m/s, 10 m/s, 15 m/s, 20 m/s and 25 m/s. Then set the tilt angle at typical angles at different speeds. The results are the forces and moments at typical speed and tilt angle. In order to get the aerodynamic interference, the isolated wing model (without rotors) simulations are set in the same condition as the control group.

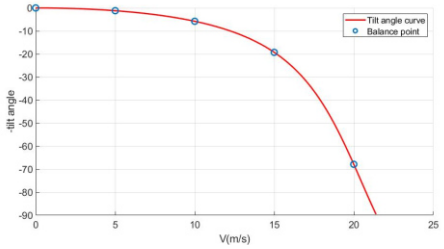

Fig. 8: Tilt angle curve

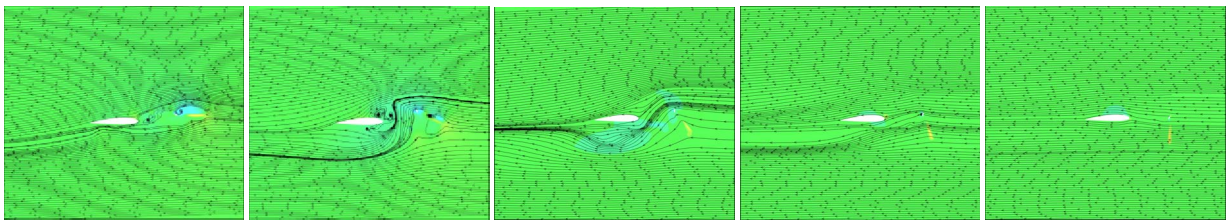

(a) Tilt angle=0,v=5m/s (b) Tilt angle=25,v=10m/s (c) Tilt angle=50,v=15m/s (d) Tilt angle=75,v=20m/s (e) Tilt angle=90,v=25m/s

Fig. 9: Pressure fields and distributions of streamlines on the wing section at different tilt angles and speed at 7000RPM

Table 2: Typical angles at different speed

Speed(m/s)	5	10	15	20	25
Angle(degree)	0-50	5-50	20-90	40-90	45-90

4.2 Result Analysis

As we know, the downwash purling generated by the rotor reduces the effective angle of attack of the wing, which causes the lift and drag of UAV to decrease. Fig.9 shows the pressure fields and distributions of streamlines on the wing at different tilt angles and speeds when the speed of the rotors is 7000 RPM. It can be seen that with the increase of the tilt angle, the negative pressure caused by the downwash purling change a lot. The central position of the negative pressure moves forward with the increase of tilt angle, at the same time, the average of negative pressure reduces. When the tilt angle is about 90 degrees, the central position of the negative pressure is beyond the wing, which causes a lift for the wing.

In order to get a numerical analysis of the aerodynamic interference, the results of the simulations for the isolated wing model and rotor/wing model are plotted in Fig.10 to Fig.12.

Fig.10 shows the curves of the lift interference respect to the tilt angle when the wind speed is at 5m/s to 25m/s. The value of interference is obtained by subtracting the lift for the isolated wing model from the lift for the rotor/wing model. It can be seen that under the aerodynamic interference, the lift of the tilt-rotor UAV decreases sharply. In the range of 0-50 degrees, as the tilt angle increases, the area of the slipstream zone caused by the wake of the rotor increases constantly, which causes the lift of the tilt-rotor UAV to decrease. When the tilt angle is greater than 50 degrees, the area of the slipstream zone no longer changes, but the effective angle of attack of the slipstream zone continues to reduce. As a result, the negative lift caused by the slipstream zone decreases. When the tilt angle is greater than 80 degrees, the effective angle of attack is small, and the slipstream zone turns to provide a positive lift.

Fig.11 shows the curves of the drag Lift interference with respect to tilt angle under different wind speeds of isolated wing model and rotor/wing modelrespect to the tilt angle when the wind speed is at 5m/s to 25m/s. The value of interference is obtained by subtracting the drag for the rotor/wing model from the drag for the rotor/wing model. It can be seen that under the aerodynamic interference, the drag of the tilt-rotor UAV decreases too. In the range of 0-50 degrees, as the tilt angle increases, the area of the slipstream zone caused

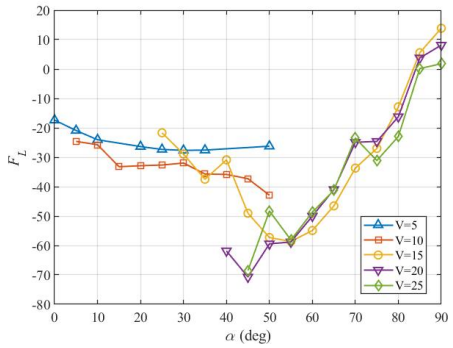

Fig. 10: Lift interference with respect to tilt angle under different wind speeds of isolated wing model and rotor/wing model

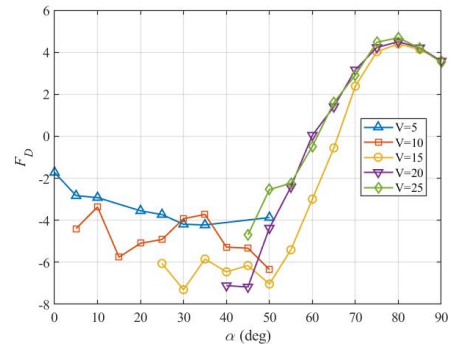

Fig. 11: Drag interference with respect to tilt angle under different wind speeds of isolated wing model and rotor/wing model

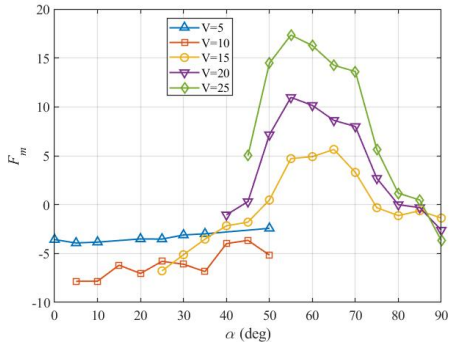

Fig. 12: Pitching moment interference with respect to tilt angle under different wind speeds of isolated wing model and rotor/wing model

by the wake of the rotor constantly increases, resulting in a decrease of the drag. Meanwhile the drag is negative and small at this time. When the tilt angle comes greater than 50 degrees, the slipstream zone no longer changes, and the effective angle of attack of the slipstream zone continues to reduce. As a result, the negative drag caused by the slipstream zone continuously decreases. When the tilt angle is greater than 60 degrees, the slipstream zone no longer provides negative drag, and the drag to the aircraft increases significantly as the tilt angle increases.

Fig.12 shows the curves of the pitching moment respect to the tilt angle when the wind speed is at 5m/s to 25m/s. The value of interference is obtained by subtracting the pitching moment for the isolated wing model from the pitching moment for the rotor/wing model. The pitching moment is a by-product of lift. The pitching moment changes due to the imbalance of lift. Within the range of 0-50 degrees, with the increase of the tilt angle, the area of the slipstream zone caused by the downwash purling continuously increased. The slipstream zone gradually expands from the leading-edge of the wing to the entire wing. As a result, the absolute value of the pitching moment decreases continuously. When the tilt angle is greater than 50 degrees, the area of the sliding zone of the wing no longer changes. As the tilt angle increases, the different degree of downwash purling attenuation causes the imbalance of the lift. The imbalanced lift leads to the direction of the pitching moment changes now. When the tilt angle is greater than 60 degrees, as the tilt angle increases, the pitching moment caused by the slipstream zone gradually decreases. When the tilt angle is greater than 75 degrees, the tilt mechanism causes a height difference between the rotor center and wing bottom. Thus, the center of the lift changes, which leads to the direction of the pitching moment change again. The effect at this time is relatively small.

The relationship between the tilt angle and the forces and moments is analyzed above. However, when taking a panoramic view of all the figures. It can be seen that the freestream influence the flow working on the wing and the downwash purling at the same time. As a result, the value of the forces and moments is related to the speed of UAV too. When the UAV flying at a low speed of about 5 m/s to 10 m/s, the combination of freestream and downwash purling is complex. Unstable flow makes the imbalance of the forces. As a result, it is hard to find out the rules of aerodynamic interference. Fortunately, the aerodynamic interference is little at that time. When it comes to the high speed at about 15m/s to 25m/s, the freestream and the downwash flow tend to be stable. Meanwhile, the aerodynamic interference comes to big. The interpolation method and fitting process can be used to describe the aerodynamic interference.

The numerical analysis above provides a way to improve the accuracy of attitude control. At the beginnging of the transition mode, the tilting speed is slow along with the speed and the effect of the aerodynamic interference is small. Meanwhile, the aerodynamic interference is less with regularity comparatively speaking. We can design a control system with strong robustness to keep the attitude stabilization. However, as the speed increases, the interference is high but regular. At the same time, the change of the tilt angle comes to fast. Simply robust control is difficult to deal with the aerodynamic interference. To solve this problem, we can turn to the rules of aerodynamic interference. More simulations are needed to find out the functional relationship between the aerodynamic interference and the speed and tilt angle. The functions translate the aerodynamic interference into compensation in the control system to keep the attitude stable. In this way, the aerodynamic interference at high speed can be restrained.

5 Conclusion

This paper analyzes the aerodynamic interference of a novel tilt-rotor UAV based on CFD. The simulation environment is set up by the hybrid grid, MRF method, $S-A$ model and Navier-Stokes equations. Furthermore, the CFD is demonstrated by comparing the simulations to the experiment. Finally, Based on the designed CFD model, the numerical simulations of rotor/wing interference is carried out, and the effect of aerodynamic interference is analyzed. According to the results, a feasible aerodynamic interference suppression strategy is suggested. Future work will be focused on the realization of the suggested control strategy by dealing with further aerodynamic interference simulations under more situations.

References

[1] K. Lu, C. Liu, C. Li, and R. Chen, "Flight dynamics modeling and dynamic stability analysis of tilt-rotor aircraft," *International Journal of Aerospace Engineering*, vol. 2019, 2019.

[2] K. Chen, Z. Shi, S. Tong, Y. Dong, and J. Chen, "Aerodynamic interference test of quad tilt rotor aircraft in wind tunnel," *Proceedings of the Institution of Mechanical Engineers, Part G: Journal of Aerospace Engineering*, p. 0954410019852827, 2019.

[3] N. T. Hegde, V. George, and C. G. Nayak, "Modelling and transition flight control of vertical take-off and landing unmanned tri-tilting rotor aerial vehicle," in *2019 3rd International conference on Electronics, Communication and Aerospace Technology (ICECA)*. IEEE, 2019, pp. 590–594.

[4] A. Akturk and C. Camci, "Tip clearance investigation of a ducted fan used in vtol uavs: Part 1 baseline experiments and computational validation," in *ASME 2011 Turbo Expo: Turbine Technical Conference and Exposition*. American Society of Mechanical Engineers, 2011, pp. 331–344.

[5] A. Vuruskan, B. Yuksek, U. Ozdemir, A. Yukselen, and G. Inalhan, "Dynamic modeling of a fixed-wing vtol uav," in *2014 International Conference on Unmanned Aircraft Systems (ICUAS)*. IEEE, 2014, pp. 483–491.

[6] P. Spalart and S. Allmaras, "A one-equation turbulence model for aerodynamic flows," in *30th aerospace sciences meeting and exhibit*, 1992, p. 439.

[7] B. Yuksek, A. Vuruskan, U. Ozdemir, M. Yukselen, and G. Inalhan, "Transition flight modeling of a fixed-wing vtol uav," *Journal of Intelligent & Robotic Systems*, vol. 84, no. 1-4, pp. 83–105, 2016.

[8] B. Wang, "Numerical simulation and analysis of helicopter rotor/fuselage flowfield based on cfd method," Ph.D. dissertation, Nanjing University of Aeronautics and Astronautics, 2007.

[9] Q. liu, "Numerical analysis on tiltrotor aircraft flowfield in hover and forward flight," Ph.D. dissertation, Nanjing University of Aeronautics and Astronautics, 2009.

[10] A. Takii, M. Yamakawa, S. Asao, and K. Tajiri, "Six degrees of freedom numerical simulation of tilt-rotor plane," in *International Conference on Computational Science*. Springer, 2019, pp. 506–519.